Supporting Information

Cazzolli et al. 10.1073/pnas.1407528111

SI Methods

Reaction Coordinate and Ratchet-and-Pawl Molecular Dynamics Algorithm. As in any variational calculation, the accuracy of the dominant reaction pathways (DRP) predictions depends on the quality of the variational space (i.e., on the algorithm used to generate the trial trajectories). To this end, we have used the following ratchet-and-pawl molecular dynamics (rMD) algorithm, which was first introduced by Paci and Karplus (1) and was further developed by Camilloni et al. (2). At each integration step, we evaluate a collective coordinate (CC), as defined by the CC z, which measures the distance between the instantaneous contact map and the native contact map:

$$z[X(t)] \equiv \sum_{i<j}^{N} \left[C_{ij}[X(t)] - C_{ij}\left(X^{\text{native}}\right)\right]^2, \qquad \textbf{[S1]}$$

where $C_{ij}(X)$ denotes the instantaneous contact map, calculated using following the equation:

$$C_{ij}(X) = \left\{1 - \left(r_{ij}/r_0\right)^6\right\} \Big/ \left\{1 - \left(r_{ij}/r_0\right)^{10}\right\}, \qquad \textbf{[S2]}$$

where $r_0 = 0.75$ nm is a characteristic reference length scale for contacts. $C_{ij}(X_{latent})$ is the contact map evaluated on the latent structure. In Eq. **S1**, the summation is restricted to atom indexes obeying $(j - i) > 35$ with a distance cutoff distance of $r_c = 1.2$ nm.

The dynamics are biased by introducing the so-called "ratchet and pawl history-dependent force":

$$\mathbf{F}_i^{bias} \equiv \begin{cases} -2k_R \nabla_i z (z - z_m(t)), & \text{if} \quad z[X(t)] > z_m(t) \\ 0, & \text{if} \quad z[X(t)] \le z_m(t). \end{cases} \qquad \textbf{[S3]}$$

where $z_m(t)$ is the minimum value assumed by the collective variable z along the trajectory, up to time t, and $k_R = 0.01$ eV is the so-called "ratchet constant." The contribution to the ratchet force due to a pair of atoms specified by the indexed i and j is set to 0 smoothly any time the distance between these atoms is larger than the cutoff distance, r_c. In this way, the computational load of the ratchet-and-pawl force scales only linearly with the number of atoms.

To weaken the effect of the bias further, we occasionally allow the system to backtrack along the direction defined by CC z. Backtracking is achieved by updating z_m when it increases according to a Metropolis accept/reject algorithm:

$$z_m' = z[X(t_{i+1})] > z_m(t_i) \quad \text{if} \quad e^{-k_a\left[0.3(z[X(t_{i+1})] - z_m(t_i)) + 2(z[X(t_i+1) - z_m(t_i))^3\right]} > x, \qquad \textbf{[S4]}$$

where $_x \in [0, 1]$ is a random number sampled from a uniform distribution and $k_a = 0.01$ is a fixed parameter that controls the acceptance ratio. Each trial trajectory consists of 5×10^4 steps of molecular dynamics with a nominal integration time step of $\Delta t = 1$ fs.

The rMD scheme efficiently generates an ensemble of trial reaction pathways while minimizing the external work applied to drive the system. In fact, when the similarity to the latent state is increasing (i.e., the number of formed latent contacts increases), the system dynamics evolve in a completely unbiased way (Eq. **S3**). Conversely, the time-dependent external force is introduced to discourage, although not to prevent completely, a similarity decrease.

Some further technical details concerning the implementation and the limitations of the DRP approach are in order. First of all, we recall that the DRPs are defined as functional minima of the Onsager–Machlup (OM) functional (Eq. **2**) and are solutions of a Newton-like second-order differential equation of motion (3). This definition implies that the dominant paths are smooth functions of time and their corresponding OM functional remains finite in the continuum limit.

One way to fulfill this condition is to use a biased Langevin equation to generate the ensemble of (nondifferentiable) trial paths and then perform a numerical relaxation of the OM action starting from each trial path, by means of some optimization algorithm [e.g., the methods used by Faccioli et al. (4) and a Beccara et al. (5)]. In such an approach, the DRP will be found by comparing the OM action for each trial path, after numerical relaxation. Unfortunately, this procedure is extremely computationally expensive for systems as large as serpins. In addition, when attempting to use this approach in atomistic protein folding simulations, we observed that the local relaxation of the trial trajectories does not lead to a significant change in the reaction mechanism but only filters out high-frequency stochastic noise in the atomic motion.

To keep the computational cost of our calculations at an affordable level, when performing the DRP simulations on large proteins, we adopt a different procedure: We generate trial trajectories using the Velocity–Verlet algorithm coupled to a Nosé–Hoover thermostat (which directly yields time-differentiable trajectories) and then rank these paths according to their OM action, without performing the local relaxation. Tests performed on different polypeptide chains have shown that neither the reaction mechanism nor the ranking of the pathways is altered by including the local relaxation of the OM.

Finally, we emphasize that any variational method is subject to uncontrolled systematic errors (i.e., it only allows identification of the "best prediction" within the considered variational model space). Hence, by enlarging the functional ensemble of trial paths, one could, in principle, find new dominant pathways with smaller OM functionals. On the other hand, in all test cases considered, we have observed that the subset of trial paths characterized by low OM values share very similar qualitative features and that the main role of the least-action principle seems to be the role of removing from the ensemble, particularly unphysical trial paths (discussion in ref. 6).

We stress again that the DRP trajectories can be used to obtain predictions for arbitrary time-independent observables, such as, for example, the rmsd to the latent structure or the fraction of native contacts. The ability to compute the reaction pathway projected on some arbitrary surface defined by the order parameters opens the door to characterizing the reaction mechanism(s).

On the other hand, the free-energy landscape; the reaction rate; and, more generally, all time-dependent observables cannot be directly inferred from the DRP algorithm, because the underlying rMD scheme accelerates the dynamics and distorts the time scale in a nonlinear manner.

Docking the Small-Molecule AZ3976 to Plasminogen Activator Inhibitor 1. The structure of the small-molecule plasminogen activator inhibitor 1 (PAI-1) inhibitor AZ3976 was taken from the crystal structure of AZ3976 bound to the latent form of PAI-1 (Protein Data Bank ID code 4AQH) (7). Docking was performed using Vina with AutoDock Tools-1.5.6 (8) and PyMOL. Docking to the active form of PAI-1 was performed using frame 1 from the

DRP trajectory. Docking to the prelatent state was performed using frame 650, which corresponds to the bottom of the initial local energy minimum (Fig. 3*A*).

Contrasting Behavior of β-Sheet A in PAI-1 vs. α_1-Antitrypin. Fig. S4 shows the structures of α_1-antitrypsin (A1AT), PAI-1 WT, and a destabilized variant of PAI-1 (PAI-1destab) in the early stage of the latency transition. Shown as spheres are positions that are highly conserved in the majority (80–95%) of serpins but not in PAI-1. Examining A1AT, it is clear that although there is separation of strand 3A (s3A) and s5A at the top of sheet A in the so-called "breach region," the center of the sheet corresponding to the shutter region resists opening. This resistance is centered on a network of conserved hydrogen bonds. This network is not present in WT PAI-1, which helps explain the fact that there is no resistance to opening in the shutter region in PAI-1, allowing for concerted separation of s3A and s5A along their entire length. Although the two mutations in PAI-1destab (G38S and Q322H) are mutations back to the serpin shutter consensus sequence (9), the DRP results show that the network of shutter interactions is still not present in this PAI-1 variant and that sheet A opening is still concerted, with no occlusion in the shutter region.

Residue Interaction Energies in the Native, Prelatent, and Latent States. Energy calculations for frames 1,650, 1,179, and 1,480 were carried out using GROMACS (10). Each frame was solvated in a box of TIP3 water and neutralized with Na^+. The system was then energy-minimized for 1,000 steps, heated to 300 K over 10 ps, and then allowed to equilibrate at 300 K for 100 ps. The average Lennard–Jones energy, Coulomb energy, and total energy of each residue were then calculated from each 100-ps simulation.

Estimating the Significance of Proposed Important Residues. The energy analysis of the active-to-prelatent transition shows that 16 residues, or 4.2% (16 of 379) of the residues, in PAI-1 contribute nearly 40% of the favorable energy for this transition. Of these residues, nine residues, or 56% of the important residues, have previously been associated with function and/or disease. How likely is it that >50% of the residues identified using an unbiased analysis of the DRP data would be disease- or function-associated?

Assuming that missense mutations are equally probable at all locations in the exons for mature PAI-1, a database containing disease-associated mutations should provide an unbiased sample pinpointing important residues. Although there is, to our knowledge, no public database of PAI-1 disease-associated missense mutations, there are databases of mutations obtained from human patients for two other human inhibitory serpins. Human mutations for A1AT are tabulated in the Leiden Open-Source Variation Database (11) (research.cchmc.org/LOVD2/home.php?select_db=SERPINA1), whereas those human mutations for antithrombin III (ATIII) are tabulated in the Imperial College, London, Antithrombin Mutation Database (www1.imperial.ac.uk/departmentofmedicine/divisions/experimentalmedicine/haematology/coag/antithrombin). These databases identify 67 and 60 disease-associated missense mutations for A1AT and ATIII, respectively, corresponding to 17% (67 of 394) and 14% (60 of 432) of the total residues in these mature serpins, respectively. This finding suggests that mutations at 15–20% of the residues in inhibitory serpins are likely to be deleterious and result in disease.

For PAI-1, 153 single residues, or 40% of the residues, in the protein have been mutated in the laboratory (12, 13). However, although some of these studies come from PAI-1 mutant libraries generated by random mutagenesis and selections for stable, functional PAI-1 variants (14–16), most of these mutations were targeted to regions believed to be important for function or folding. Thus, this group is not an unbiased collection of PAI-1 mutations. Nonetheless, of these 153 mutations, mutations at 102 positions, or 27% (102 of 379) of the total residues in PAI-1, have deleterious or beneficial effects, making it possible that mutations at 27–30% of the residues in PAI-1 will affect function or folding. Note that 30% is likely an overestimate due to the targeted nature of most of the PAI-1 mutations.

Thus, we would expect that randomly choosing 16 residues from mature PAI-1 would yield two (13%) to five (31%) residues previously identified as important for folding or function in inhibitory serpins. Thus, our finding that 9 of 16 residues, or 56% of the residues, we identified as energetically important for the active-to-prelatent transition have also been previously identified as important for function or folding is statistically significant. This result further supports the use of the DRP method to identify important residues, providing insight into the function of serpins and other proteins.

1. Paci E, Karplus M (1999) Forced unfolding of fibronectin type 3 modules: An analysis by biased molecular dynamics simulations. *J Mol Biol* 288(3):441–459.
2. Camilloni C, Broglia RA, Tiana G (2011) Hierarchy of folding and unfolding events of protein G, CI2, and ACBP from explicit-solvent simulations. *J Chem Phys* 134(4): 045105.
3. Sega M, Faccioli P, Pederiva F, Garberoglio G, Orland H (2007) Quantitative protein dynamics from dominant folding pathways. *Phys Rev Lett* 99(11):118102.
4. Faccioli P, Sega M, Pederiva F, Orland H (2006) Dominant pathways in protein folding. *Phys Rev Lett* 97(10):108101.
5. a Beccara S, Škrbić T, Covino R, Micheletti C, Faccioli P (2013) Folding pathways of a knotted protein with a realistic atomistic force field. *PLoS Comput Biol* 9(3):e1003002.
6. a Beccara S, Škrbić T, Covino R, Faccioli P (2012) Dominant folding pathways of a WW domain. *Proc Natl Acad Sci USA* 109(7):2330–2335.
7. Fjellström O, et al. (2013) Characterization of a small molecule inhibitor of plasminogen activator inhibitor type 1 that accelerates the transition into the latent conformation. *J Biol Chem* 288(2):873–885.
8. Trott O, Olson AJ (2010) AutoDock Vina: Improving the speed and accuracy of docking with a new scoring function, efficient optimization, and multithreading. *J Comput Chem* 31(2):455–461.
9. Hansen M, Busse MN, Andreasen PA (2001) Importance of the amino-acid composition of the shutter region of plasminogen activator inhibitor-1 for its transitions to latent and substrate forms. *Eur J Biochem* 268(23):6274–6283.
10. Hess B, Kutzner C, van der Spoel D, Lindahl E (2008) GROMACS 4: Algorithms for highly efficient, load-balanced, and scalable molecular simulation. *J Chem Theory Comput* 4:435–447.
11. Fokkema IFAC, et al. (2011) LOVD v.2.0: The next generation in gene variant databases. *Hum Mutat* 32(5):557–563.
12. De Taeye B, Gils A, Declerck PJ (2004) The story of the serpin plasminogen activator inhibitor 1: Is there any need for another mutant? *Thromb Haemost* 92(5):898–924.
13. Lin Z, et al. (2013) Structural insight into inactivation of plasminogen activator inhibitor-1 by a small-molecule antagonist. *Chem Biol* 20(2):253–261.
14. Berkenpas MB, Lawrence DA, Ginsburg D (1995) Molecular evolution of plasminogen activator inhibitor-1 functional stability. *EMBO J* 14(13):2969–2977.
15. Stoop AA, Jespers L, Lasters I, Eldering E, Pannekoek H (2000) High-density mutagenesis by combined DNA shuffling and phage display to assign essential amino acid residues in protein-protein interactions: Application to study structure-function of plasminogen activation inhibitor 1 (PAI-I). *J Mol Biol* 301(5):1135–1147.
16. Stoop AA, Eldering E, Dafforn TR, Read RJ, Pannekoek H (2001) Different structural requirements for plasminogen activator inhibitor 1 (PAI-1) during latency transition and proteinase inhibition as evidenced by phage-displayed hypermutated PAI-1 libraries. *J Mol Biol* 305(4):773–783.

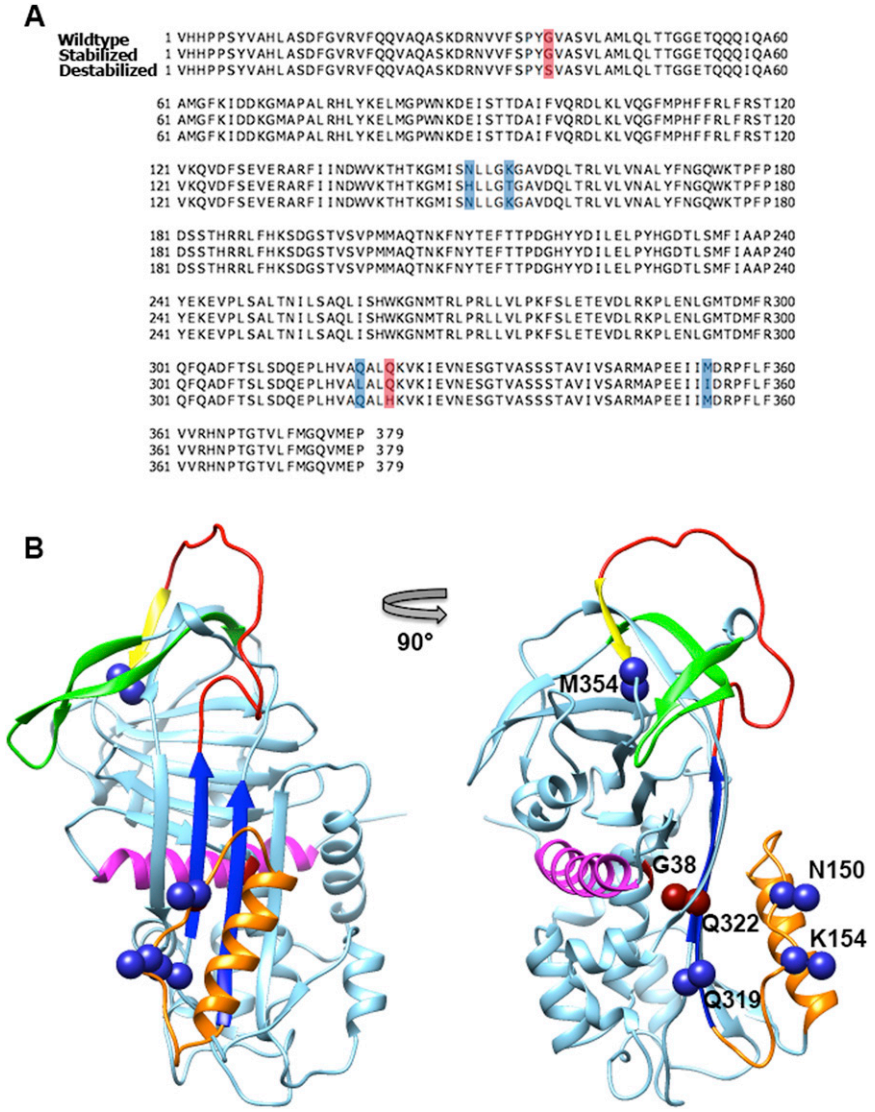

Fig. S1. PAI-1 amino acid sequences and stability-altering mutations. (*A*) PAI-1 sequences used for the DRP simulations. The locations of stabilizing and destabilizing mutations are indicated in blue and red, respectively. (*B*) Active PAI-1 structure showing the locations of stabilizing (blue, $n = 4$) and destabilizing (red, $n = 2$) mutations in PAI-1stab and PAI-1destab, respectively. The gate is shown in green; s1C is shown in yellow; the reactive center loop (RCL) is shown in red; helices A and F are shown in magenta and orange, respectively; and s3A and s5A are shown in dark blue. The C_α and C_β atoms of stabilizing and destabilizing mutated residues are shown as spheres.

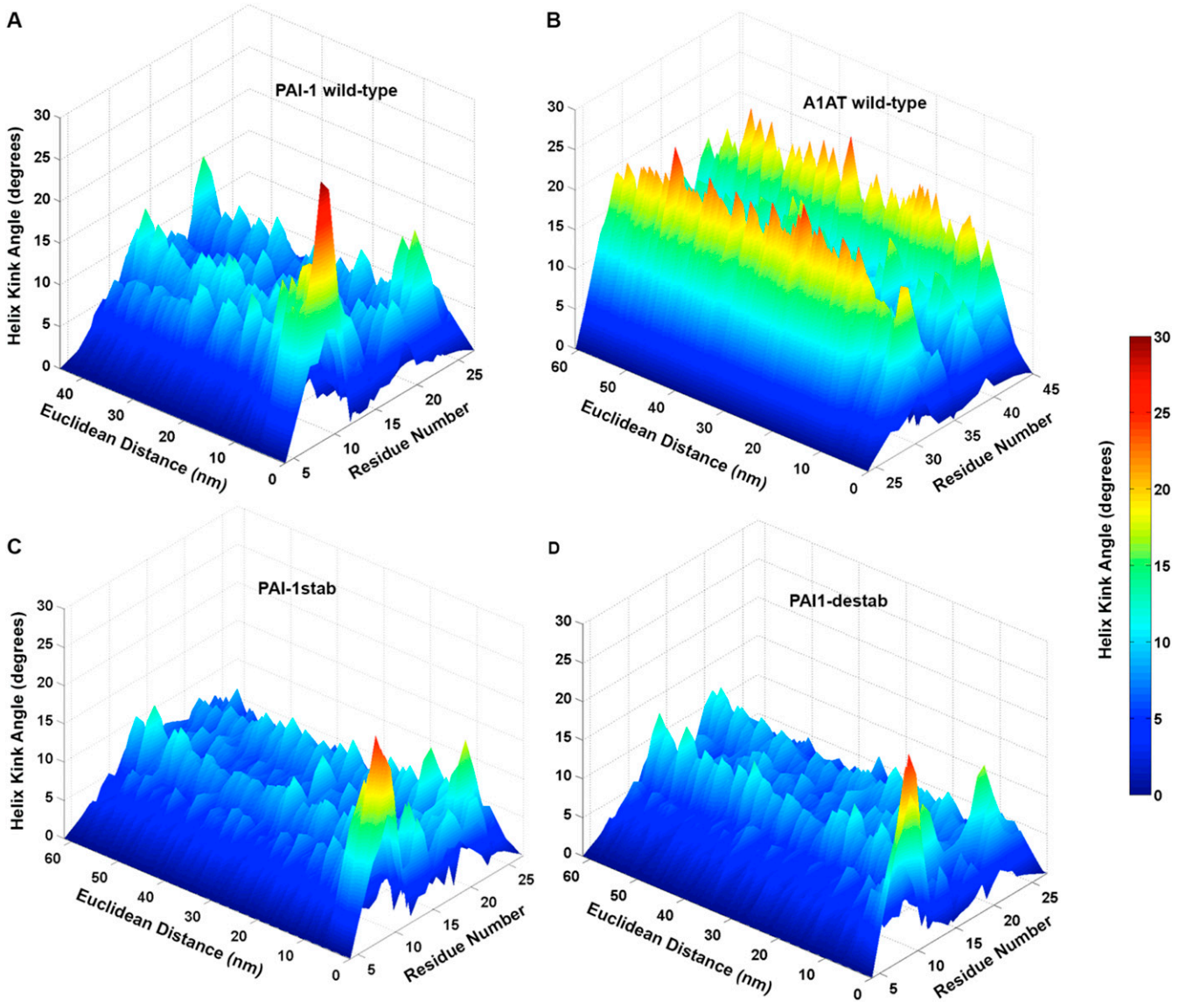

Fig. S2. Transition from active to prelatent relaxes the kink in helix A. The 20–30° kink at the N terminus of helix A is relaxed upon transitioning to the prelatent state for WT PAI-1 (*A*), PAI-1stab (*C*), and PAI-1destab (*D*). (*B*) No significant changes in kink angles are observed for WT A1AT. Kink angles were calculated along the DRP trajectories using Bendix (1). PAI-1 helix A was defined from Pro4 to Ser27 (PAI-1 numbering), whereas A1AT helix A was defined from Asn24 to Ser45 (A1AT numbering). Changes to the helix start and end altered the value of the angles but not the trend.

1. Dahl ACE, Chavent M, Sansom MSP (2012) Bendix: Intuitive helix geometry analysis and abstraction. *Bioinformatics* 28(16):2193–2194.

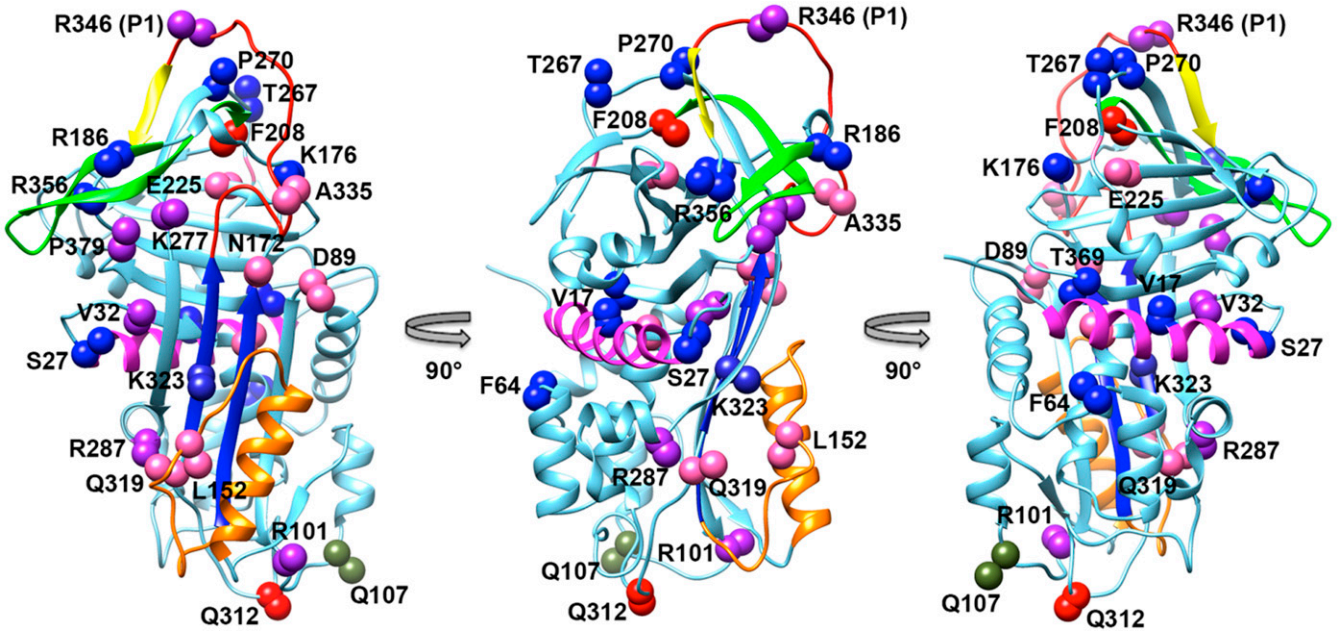

Fig. S3. Locations of the energetically important residues listed in Table S1. The gate is shown in green; s1C is shown in yellow; the RCL is shown in red; helices A and F are shown in magenta and orange, respectively; and s3A and s5A are shown in dark blue. The C_α and C_β atoms of the energetically important residues are shown as spheres. The residues are colored according to the energetics of the active-to-prelatent (A to PL) and PL-to-higher energy (PL to HE) transitions as follows: blue, favorable A to PL and unfavorable PL to HE; purple, favorable A to PL and not significant (NS) for PL to HE; pink, unfavorable A to PL and NS for PL to HE; red, unfavorable A to PL and favorable PL to HE; green, NS for A to PL and favorable PL to H.

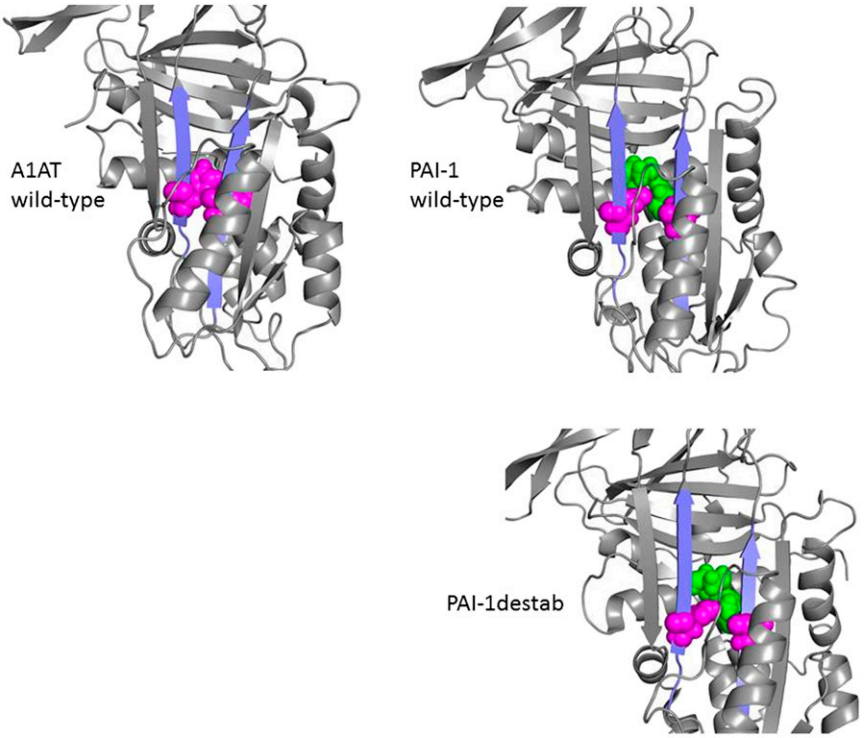

Fig. S4. β-Strands 3A and 5A (blue) during the early stages of the latency transition for WT A1AT, WT PAI-1, and PAI-1destab. The shutter region, shown in green and magenta spheres, contains a network of interacting residues that are highly conserved in serpins (1, 2). These residues help keep the bottom of sheet A closed, as observed in the A1AT latency transition. A1AT contains the conserved sequence Ser56 in helix B (green) and Asn186 and His334 in s3A and s5A (magenta), respectively. In WT PAI-1, the serine residue in helix B is a glycine, Gly38 (green), and the histidine residue in s3A is a glutamine, Gln322 (magenta), whereas the Asn residue in s3A (magenta) is conserved. In PAI-1destab, these residues are reverted back to the consensus sequence, G38S and Q322H, but the DRP results show that this change is not sufficient to reconstitute the packing of the shutter and sheet A still opens all of the way early in the latency transition.

1. Hansen M, Busse MN, Andreasen PA (2001) Importance of the amino-acid composition of the shutter region of plasminogen activator inhibitor-1 for its transitions to latent and substrate forms. *Eur J Biochem* 268(23):6274–6283.
2. Irving JA, Pike RN, Lesk AM, Whisstock JC (2000) Phylogeny of the serpin superfamily: Implications of patterns of amino acid conservation for structure and function. *Genome Res* 10(12): 1845–1864.

Table S1. Mutating residues identified as energetically important for the active (A)-to-prelatent (PL) or PL-to–high-energy state (HE) conformational change are often deleterious

PAI-1 residue (location)	Energetic contribution, A to PL*	Energetic contribution, PL to HE*	Effects of mutations[†,‡]
Val17 (hA)	Favorable	Unfavorable	Some mutations reduce activity (1).
Ser27 (turn hA to s6B)	Favorable	Unfavorable	Reported mutations are nonperturbing (2).
Val32 (s6B)	Favorable	NS	This residue is in the shutter region. Although no mutations are reported at this exact location, mutations at residues 33–34 (50–52 using the A1AT numbering) are associated with serpin polymerization and disease (reviewed in ref. 3).
Tyr37 (hB)	Unfavorable	NS	In PAI-1, mutations to the preceding residues, Pro36, increase the functional $t_{1/2}$ (4). In α_1-antichymotrypsin, mutations at this site lead to low levels in plasma and disease (5, 6).
Phe64 (loop hC to hD)	Favorable	Unfavorable	No reported mutations
Asp89 (N terminus to s2A)	Unfavorable	NS	No reported mutations; part of the binding epitope for the antibody 33B8 that increases the latency rate (7)
Arg101 (C terminus to s2A)	Favorable	NS	This residue is a highly conserved arginine residue in 98% of PAI-1 sequences. Arg101 is important for vitronectin binding (8).
Gln107 (loop s2A to hE)	NS	Favorable	No reported mutations
Leu152 (loop from hF to s3A)	Unfavorable	NS	No reported mutations. Although no mutations are reported at Leu152, this loop is important for reactive center loop (RCL) insertion and mutations in this loop often have functional consequences (4, 9).
Asn172 (N terminus to s3A)	Unfavorable	NS	No reported mutations
Lys176 (loop s3A to sheet C)	Favorable	Unfavorable	Deleterious effects on stability in the serpin thyroxine-binding globulin (6, 10)
Arg186 (s4C, gate)	Favorable	Unfavorable	Deleterious, effects on PAI-1 $t_{1/2}$ (11, 12)
Phe208 (s3C)	Unfavorable	Favorable	No reported mutations; Phe208 is adjacent to the Asn209 glycosylation site in PAI-1, and glycosylation may affect the RCL conformation (13).
Glu225 (s2B)	Unfavorable	NS	Mutating to Lys results in a $t_{1/2}$ of minutes (14).
Gly264 (loop hH to s2C)	Unfavorable	NS	No reported mutations; this residue is adjacent to the glycosylation site at Asn265, and glycosylation may affect the RCL conformation (13).
Thr267 (loop hG to s2C)	Favorable	Unfavorable	No reported mutations
Pro270 (s2C)	Favorable	Unfavorable	Mutating to Cys is nonperturbing (15).
Lys277 (loop s2C to s6A)	Favorable	NS	Deleterious, effects on folding in A1AT (16, 17); Lys or Arg in most serpin sequences
Arg287 (hI)	Favorable	NS	Deleterious, effects on folding, stability, and activity for A1AT (18)
Gln312 (loop hI to s5A)	Unfavorable	Favorable	No reported mutations
Gln319 (loop hI to s5A)	Unfavorable	NS	Gln319Leu mutation helps stabilize active PAI-1 (4).
Lys323 (s5A)	Favorable	Unfavorable	Usually Lys in PAI-1 and other serpins; Lys323Ala stabilizes active PAI-1 in the absence of vitronectin (19); deleterious effects on protease inhibition in PAI-1 and other serpins (18, 20, 21)
Ala335 (P12 in RCL)	Unfavorable	NS	This residue is in the hinge region and is highly conserved in serpins. Ala335Pro is a protease substrate rather than an inhibitor (22).
Arg346 (P1 in RCL)	Favorable	NS	This residue is the P1 residue in the RCL (i.e., the residue N-terminal to the protease cleavage site). This residue is therefore important for protease specificity.
Arg356 (loop s1C to s4B)	Favorable	Unfavorable	This residue is in the distal hinge region, which is important for conformational changes. Mutations have deleterious effects on folding and $t_{1/2}$ (23).
Thr369 (loop s4B to s5B)	Favorable	Unfavorable	No reported mutations
Pro379 (C terminus)	Favorable	NS	This Pro residue is very conserved among serpins, with deleterious effects on activity and folding in a variety of serpins (6, 24–28).

h, helix; NS, not significant; s, strand.

*Energies were determined from molecular dynamics simulations beginning from frame 1 (active) or frame 650 (prelatent) extracted from the DRP simulation. These frames were equilibrated, and energies were extracted as described in *SI Methods*. Favorable and unfavorable changes in energetic contributions were identified using an energy cutoff in units of thermal energy (k_BT) of -40 k_BT and $+40$ k_BT, respectively.

[†]Effects of mutations were primarily determined from the PAI-1 literature and corroborated by reported mutations for other serpins. Corresponding mutations in other serpins were found by structurally aligning the first frame used for the DRP simulations with the following X-ray crystal structures from the Protein Data Bank (PDB): ID code 1qlp for A1AT (29), ID code 1qmn for α_1-antichymotrypsin (30), ID code 1e05 for ATIII (31), and ID code 2ceo for thyroxine-binding globulin (32).

[‡]Comprehensive list of PAI-1 mutations is provided in a review by De Taeye et al. (33). More general lists of serpin mutations are provided by Gooptu and Lomas (3) and Stein and Carrell (6).

1. Seo EJ, Im H, Maeng JS, Kim KE, Yu MH (2000) Distribution of the native strain in human α_1-antitrypsin and its association with protease inhibitor function. *J Biol Chem* 275(22): 16904–16909.
2. UniProt Consortium (2014) Activities at the universal protein resource (UniProt). *Nucleic Acids Res* 42(Database issue):D191–D198.

3. Gooptu B, Lomas DA (2009) Conformational pathology of the serpins: Themes, variations, and therapeutic strategies. *Annu Rev Biochem* 78:147–176.
4. Berkenpas MB, Lawrence DA, Ginsburg D (1995) Molecular evolution of plasminogen activator inhibitor-1 functional stability. *EMBO J* 14(13):2969–2977.
5. Poller W, et al. (1993) A leucine-to-proline substitution causes a defective α1-antichymotrypsin allele associated with familial obstructive lung disease. *Genomics* 17(3):740–743.
6. Stein PE, Carrell RW (1995) What do dysfunctional serpins tell us about molecular mobility and disease? *Nat Struct Biol* 2(2):96–113.
7. Gorlatova NV, Elokdah H, Fan K, Crandall DL, Lawrence DA (2003) Mapping of a conformational epitope on plasminogen activator inhibitor-1 by random mutagenesis. Implications for serpin function. *J Biol Chem* 278(18):16329–16335.
8. Jensen JK, et al. (2004) Construction of a plasminogen activator inhibitor-1 variant without measurable affinity to vitronectin but otherwise normal. *FEBS Lett* 556(1-3):175–179.
9. Wind T, Jensen JK, Dupont DM, Kulig P, Andreasen PA (2003) Mutational analysis of plasminogen activator inhibitor-1. *Eur J Biochem* 270(8):1680–1688.
10. Takeda K, et al. (1989) Sequence of the variant thyroxine-binding globulin of Australian aborigines. Only one of two amino acid replacements is responsible for its altered properties. *J Clin Invest* 83(4):1344–1348.
11. Gils A, Lu J, Aertgeerts K, Knockaert I, Declerck PJ (1997) Identification of positively charged residues contributing to the stability of plasminogen activator inhibitor 1. *FEBS Lett* 415(2): 192–195.
12. Bijnens AP, et al. (2001) The distal hinge of the reactive site loop and its proximity: A target to modulate plasminogen activator inhibitor-1 activity. *J Biol Chem* 276(48):44912–44918.
13. Gils A, et al. (2003) Biochemical importance of glycosylation of plasminogen activator inhibitor-1. *Thromb Haemost* 90(2):206–217.
14. Sui G-C, Wiman B (2000) The Bβ-sheet in the PAI-1 molecule plays an important role for its stability. *Thromb Haemost* 83(6):896–901.
15. De Taeye B, Compernolle G, Dewilde M, Biesemans W, Declerck PJ (2003) Immobilization of the distal hinge in the labile serpin plasminogen activator inhibitor 1: Identification of a transition state with distinct conformational and functional properties. *J Biol Chem* 278(26):23899–23905.
16. Brantly M, Courtney M, Crystal RG (1988) Repair of the secretion defect in the Z form of α1-antitrypsin by addition of a second mutation. *Science* 242(4886):1700–1702.
17. Lomas DA, Evans DL, Finch JT, Carrell RW (1992) The mechanism of Z α_1-antitrypsin accumulation in the liver. *Nature* 357(6379):605–607.
18. Knaupp AS, et al. (2013) The roles of helix I and strand 5A in the folding, function and misfolding of α1-antitrypsin. *PLoS ONE* 8(1):e54766.
19. Hansen M, Busse MN, Andreasen PA (2001) Importance of the amino-acid composition of the shutter region of plasminogen activator inhibitor-1 for its transitions to latent and substrate forms. *Eur J Biochem* 268(23):6274–6283.
20. Im H, Yu MH (2000) Role of Lys335 in the metastability and function of inhibitory serpins. *Protein Sci* 9(5):934–941.
21. Kirkegaard T, et al. (1999) Engineering of conformations of plasminogen activator inhibitor-1. A crucial role of β-strand 5A residues in the transition of active form to latent and substrate forms. *Eur J Biochem* 263(2):577–586.
22. Audenaert AM, Knockaert I, Collen D, Declerck PJ (1994) Conversion of plasminogen activator inhibitor-1 from inhibitor to substrate by point mutations in the reactive-site loop. *J Biol Chem* 269(30):19559–19564.
23. Wang Q, Shaltiel S (2003) Distal hinge of plasminogen activator inhibitor-1 involves its latency transition and specificities toward serine proteases. *BMC Biochem* 4:5.
24. Olds RJ, et al. (1992) Antithrombin III Budapest: A single amino acid substitution (429Pro to Leu) in a region highly conserved in the serpin family. *Blood* 79(5):1206–1212.
25. Mille B, Watton J, Barrowcliffe TW, Mani JC, Lane DA (1994) Role of N- and C-terminal amino acids in antithrombin binding to pentasaccharide. *J Biol Chem* 269(47):29435–29443.
26. Eldering E, Verpy E, Roem D, Meo T, Tosi M (1995) COOH-terminal substitutions in the serpin C1 inhibitor that cause loop overinsertion and subsequent multimerization. *J Biol Chem* 270(6):2579–2587.
27. Verpy E, et al. (1995) Crucial residues in the carboxy-terminal end of C1 inhibitor revealed by pathogenic mutants impaired in secretion or function. *J Clin Invest* 95(1):350–359.
28. Fra AM, et al. (2012) Three new alpha1-antitrypsin deficiency variants help to define a C-terminal region regulating conformational change and polymerization. *PLoS ONE* 7(6):e38405.
29. Elliott PR, Pei XY, Dafforn TR, Lomas DA (2000) Topography of a 2.0 A structure of α_1-antitrypsin reveals targets for rational drug design to prevent conformational disease. *Protein Sci* 9(7):1274–1281.
30. Gooptu B, et al. (2000) Inactive conformation of the serpin $\alpha(_1)$-antichymotrypsin indicates two-stage insertion of the reactive loop: Implications for inhibitory function and conformational disease. *Proc Natl Acad Sci USA* 97(1):67–72.
31. McCoy AJ, Pei XY, Skinner R, Abrahams JP, Carrell RW (2003) Structure of β-antithrombin and the effect of glycosylation on antithrombin's heparin affinity and activity. *J Mol Biol* 326 (3):823–833.
32. Zhou A, Wei Z, Read RJ, Carrell RW (2006) Structural mechanism for the carriage and release of thyroxine in the blood. *Proc Natl Acad Sci USA* 103(36):13321–13326.
33. De Taeye B, Gils A, Declerck PJ (2004) The story of the serpin plasminogen activator inhibitor 1: Is there any need for another mutant? *Thromb Haemost* 92(5):898–924.

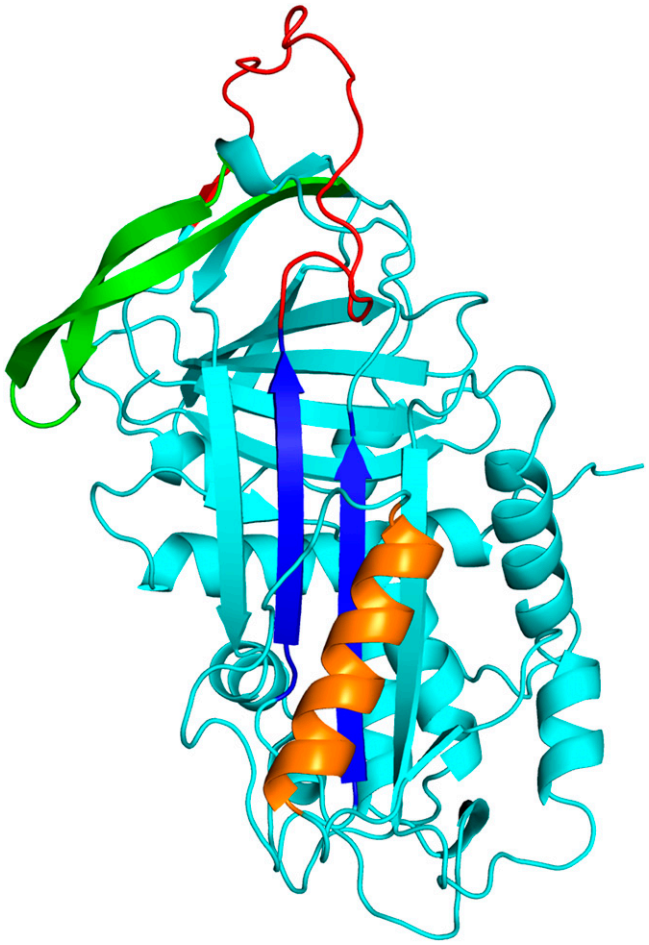

Movie S1. The trajectory of the active → latent transition for wild-type PAI-1 computed from DRP simulations. Structural elements are colored as in Fig. 1.

Movie S1

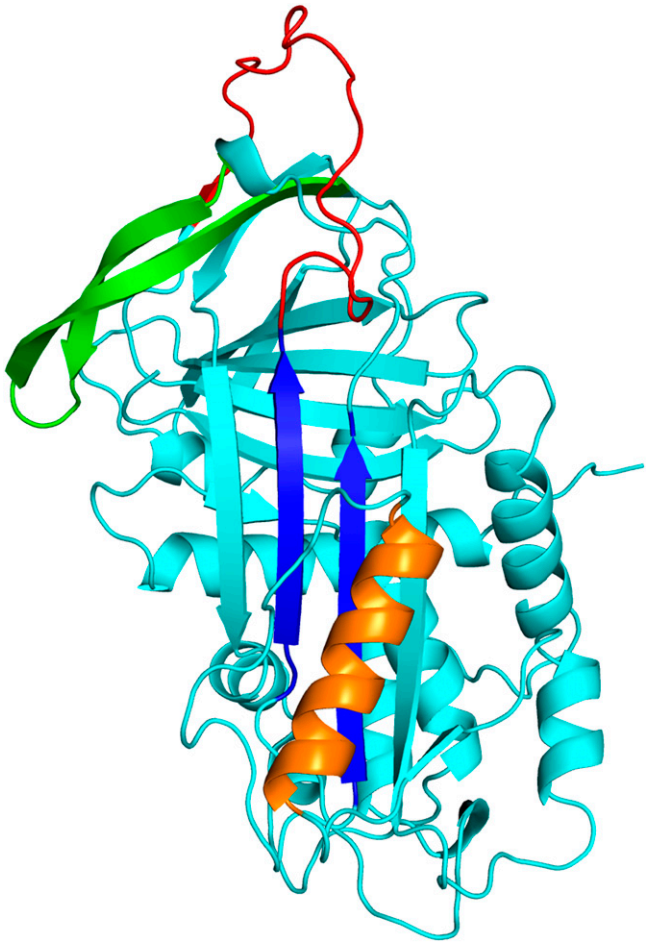

Movie S2. The trajectory of the active → latent transition for the mutant PAI-1destab computed from DRP simulations. Structural elements are colored as in Fig. 1.

Movie S2

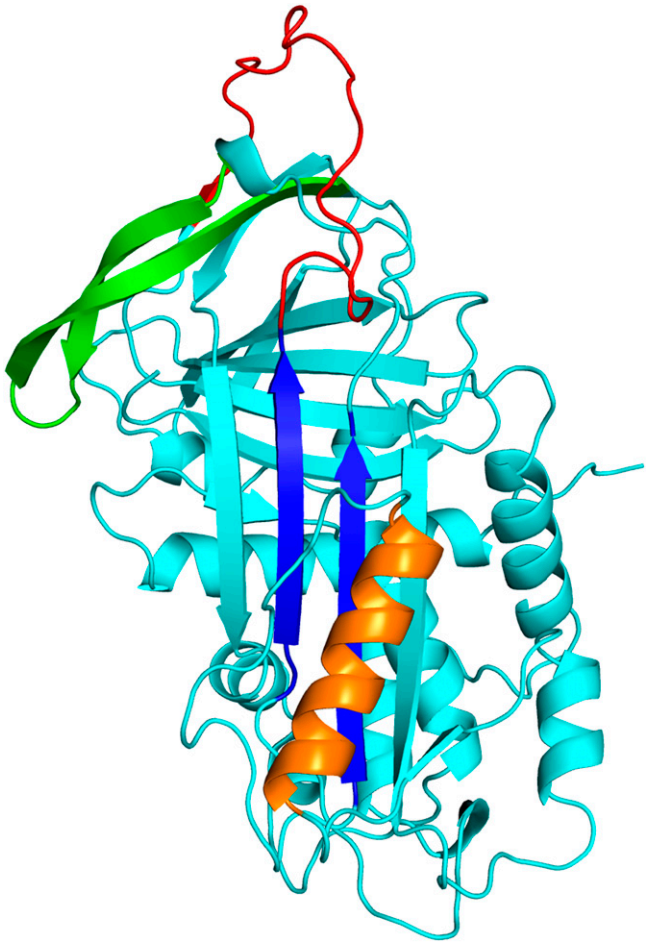

Movie S3. The trajectory of the active → latent transition for the mutant PAI-1stab computed from DRP simulations. Structural elements are colored as in Fig. 1.

Movie S3

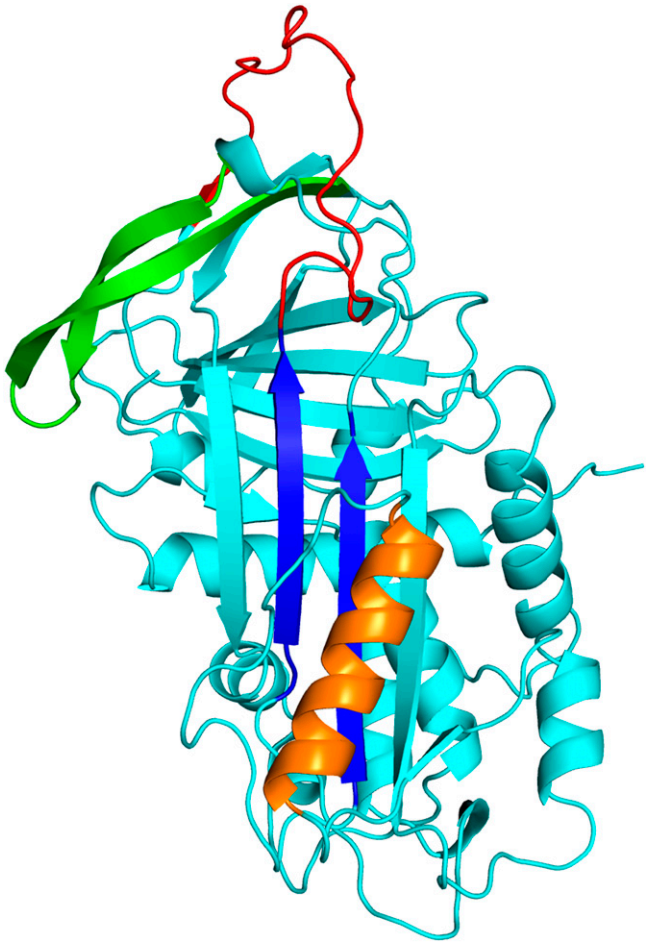

Movie S4. The trajectory of the active → latent transition for wild-type A1AT computed from DRP simulations. Structural elements are colored as in Fig. 1.

Movie S4